17

High Resolution X-Ray Tomography - 3D Imaging for Tissue Engineering Applications

Zehbe Rolf *, Haibel Astrid, Schmidt Franziska, Riesemeier Heinrich, Kirkpatrick C. James, Schubert Helmut and Brochhausen Christoph
Technische Universität Berlin, Institute of Materials Science and Technologies
Germany

1. Introduction

Synchrotron radiation-based micro computed tomography (SR-μCT) has become a valuable tool for the structural analyzes of different types of biomaterials in tissue engineering research. This methodology allows to investigate millimetre sized specimens in their three dimensional context - even on a cellular level without destroying the material.
In this chapter we elucidate the use of SR-μCT to analyze several biomaterials for tissue engineering research, which are targeted at different applications in the life sciences and which feature completely different properties. Among the investigated materials are biopolymeric scaffolds for cartilage tissue engineering, a commercial fibre based scaffold, biodegradable microspheres as drug release system and two multi-layered materials for possible applications in guided nerve growth. Further, as the used SR-μCT beam line allows the generation of coherent and monochromatic X-rays, limitations due to low differences in absorption contrast can be solved by using the enhanced phase contrast imaging capabilities of the beam line station. The three-dimensional data acquired for each investigated sample allowed for qualitative and quantitative results unprecedented by light microscopy or electron microscopy. While the main focus has been set on imaging aspects, the results obtained are discussed in view of the respective literature indicating trends in future research.

*Author for correspondence: Rolf Zehbe (rolf.zehbe@tu-berlin.de), other authors affiliations as follows:
Zehbe, Schmidt & Schubert: TU Berlin, Institute of Materials Science & Technologies, Englische Strasse 20, 10587 Berlin, Germany
Haibel: GKSS Research Centre at DESY, Petra III, Notkestrasse 85, 22607 Hamburg, Germany
Riesemeier: BAM, Federal Institute for Materials Research & Testing, Division I.3, Richard Willstätter Strasse 11, 12489 Berlin, Germany
Brochhausen & Kirkpatrick: Johannes Gutenberg University, Institute of Pathology, Langenbeckstrasse 1, 55101 Mainz, Germany

2. Fundamentals of X-Ray Imaging and Tomography

In 1895 Wilhelm Conrad Röntgen discovered a new type of radiation being emitted from a vacuum tube while investigating cathode rays (Röntgen, 1895). Röntgen named this type of radiation X-rays and produced the first medical X-ray image showing his wife's hand. X-rays are part of the electromagnetic spectrum, although with a much shorter wavelength than visible light and with the ability to penetrate matter depending on atomic mass (μ) and density (respectively the thickness d) according to the Lambert-Beer's law (1).
Especially biological matter, being of low density and being mostly composed of elements with a low atomic mass, is penetrated rather well. Consequently, the application of X-rays to medical sciences was established from the very beginning, but soon extended to applications in chemistry, physics and materials sciences.

$$I = I_0 e^{-\mu d} \tag{1}$$

Just over twenty years later in 1917 Johann Radon (Radon, 1917) developed the mathematical base to calculate cross-sectional views from series of rotational projection images - an approach which ultimately laid the basis for X-ray tomography and which is known as the projection-slice theorem. Simplified, the projection image of an object at a certain rotation angle $\boldsymbol{\theta}$ can be described as a set of line integrals, which themselves represent the attenuation of the X-ray after traversal through the object. This intensity information is, like the first X-ray image of Röntgen's wife, a two-dimensional image. Following, the mathematical fundamentals to derive three-dimensional data from these sets of projection images in parallel beam geometry are briefly summarized. Although, other beam geometries, like conical or fan beams exist, the simplest mathematical approach is given considering a parallel beam of X-rays. This setup was furthermore exclusively used in all experiments described in this chapter. For a more in depth description, the reader is referred to the work of Kak and Slaney (Kak & Slaney, 1988). Briefly, the total attenuation $\boldsymbol{p}$ of a ray at an angle $\boldsymbol{\theta}$ and a position $\boldsymbol{r}$ relative to the rotation centre as displayed for a phantom object in Figure 1a is given by equation (2), where $\boldsymbol{I}$ is the intensity and $\boldsymbol{\mu}$ is the attenuation coefficient corresponding to the Lambert-Beer's law.

$$p(r,\theta) = \ln(I / I_0) = -\int \mu(x,y) ds \tag{2}$$

Consequently, a point (x,y) is projected onto $r(\boldsymbol{\theta})$ according to equation (3).

$$r = x\cos\theta + y\sin\theta \tag{3}$$

Using above formula, equation (2) can be rewritten in its transformed form (4), which is called the radon transform or sinogram (Figure 1b).

$$p(r,\theta) = \int_{-\infty}^{\infty}\int_{-\infty}^{\infty} f(x,y)\delta(x\cos\theta + y\sin\theta - r)dxdy \tag{4}$$

In tomography, the sinogram is used to reconstruct the sliced data from the projection data via the inverse of equation (4). The exact reconstruction of a given object in its sliced form requires an infinite amount of projections due to the projection-slice theorem.
Practically, a finite amount of projections in the range of 10^3 is used to optimize between data size/ processing time and reconstructed details.
Figure 1c displays the back projection obtained from the sinogram, which appears blurred and features a distinct halo. Applying a filter significantly reduces this effect and is consequently termed filtered back projection (Figure 1d, some artefacts can be observed as displayed in the cut-out). A parallel beam geometry has another favourable impact on the reconstruction of tomographic data as projections from 0°-180° are identical to projections from 180°-360°, which is, for example, not the case for a conical or fan beam geometry. This reduced amount of needed measurements directly impacts computing time and data size.

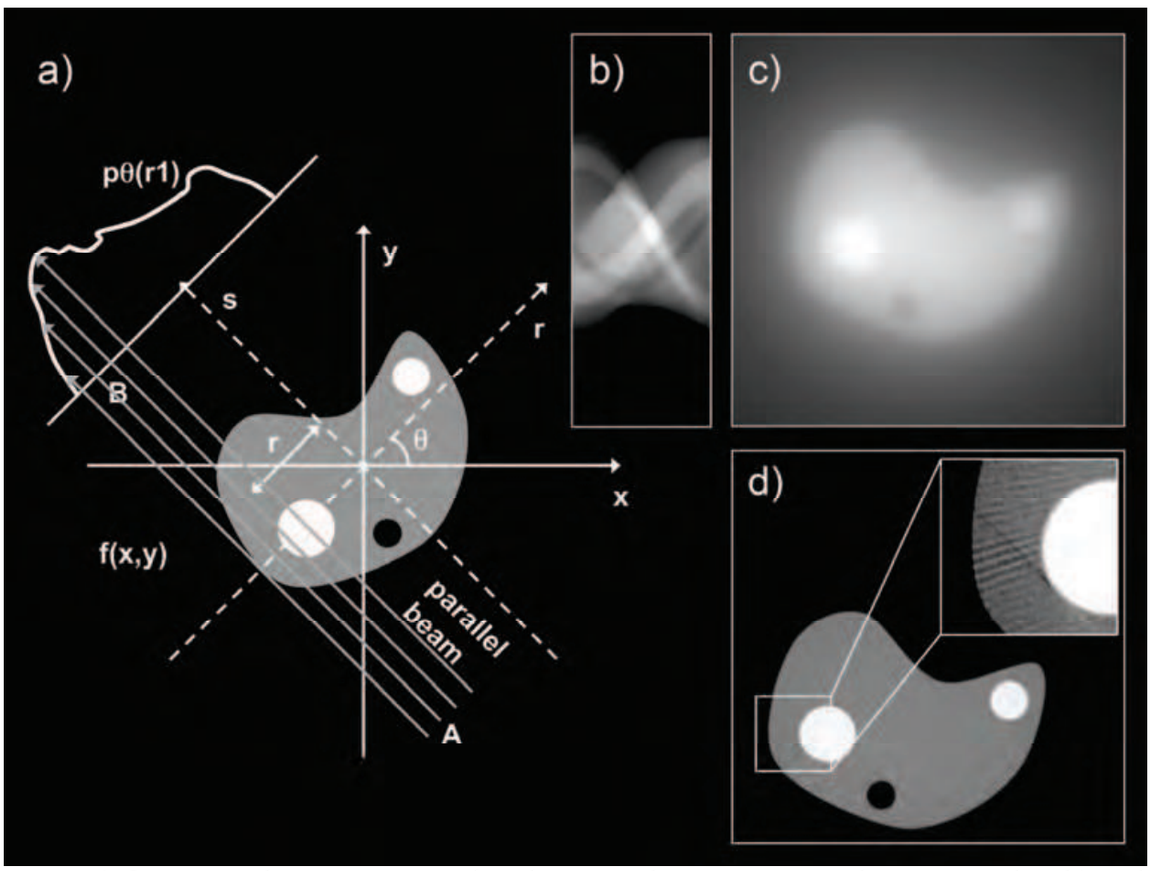

Fig. 1. a) Geometrical representation for obtaining the sinogram as demonstrated in b) and which is back projected as shown in c) without applying filtering and d) applying a ramp filter (the cut-out has been enhanced in contrast to display artefacts due to reconstruction).

3. Synchrotrons as Source for Superior X-Rays

X-rays can be produced in two different ways. The first approach dates back to Röntgen and uses X-ray tubes, essentially evacuated glass tubes with an electrically heated cathode,

which emits electrons by thermionic emission from e.g. a tungsten filament. These electrons are accelerated towards the anode (e.g. copper) by applying a high voltage in the range of some kilovolts to hundred kilovolts. Furthermore, the anode's plain surface is positioned at an angle relative to the incident electrons at around 5° to 20° and it is made of a heat resistant material like tungsten or molybdenum as most of the energy is dissipated as heat upon deceleration of the electrons in the anode material. Only a few percent of the energy is converted into X-rays which are emitted as a fan or cone beam.

Although, current X-ray tube-based experimental setups can achieve high quality scientific data, some beam related limitations cannot be resolved. Here, synchrotrons offer a more advanced source for X-rays by accelerating charged particles (e.g. electrons) in storage rings up to relativistic speeds. Although electromagnetic radiation (or synchrotron radiation) is already emitted tangentially solely due to the particles being accelerated on a circular pathway, the efficacy can be raised significantly using undulators or wigglers. These so called insertion devices produce forward directed synchrotron radiation by using a series of alternating magnets, forcing the particles into oscillations and to loose energy in the form of synchrotron radiation. This radiation offers a high photon flux over a large range of energies, a high brilliance, a high level of polarization and coherency. Due to the high photon flux, wavelength monochromatization is a feasible approach (Dilmanian, 1992; Bonse & Bush, 1996). In this context, methods based on synchrotron radiation, allow for faster measurements and a broader spectrum of applications. For a more detailed comparison between synchrotron generated and tube-generated X-rays, the reader is referred to Bernhard et al. (Bernhard et al., 2004).

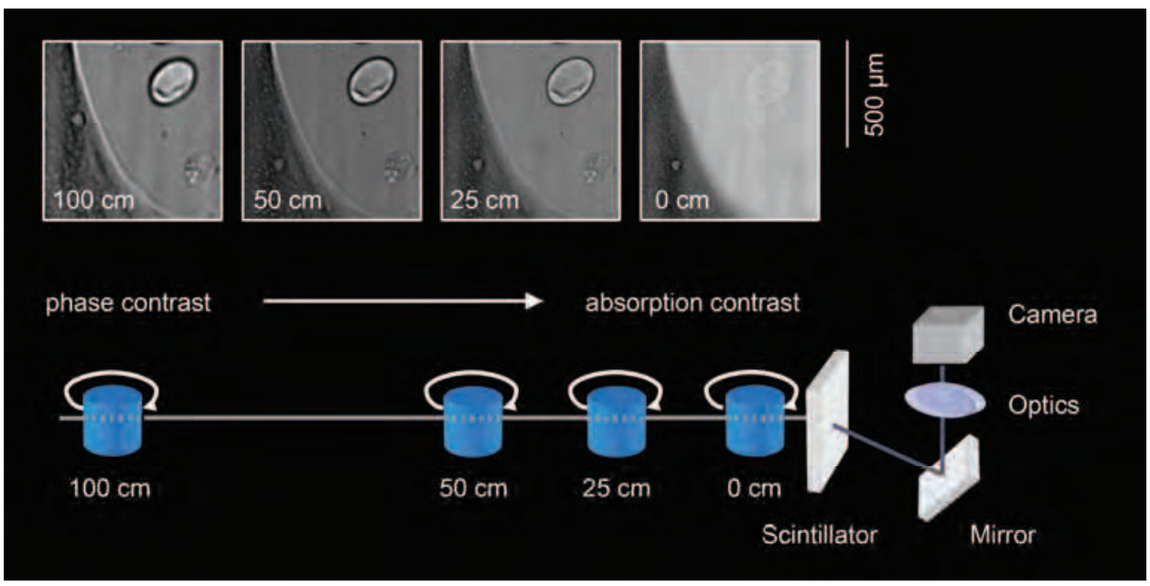

Fig. 2. Basic SR-µCT experimental setup, allowing measurement in both absorption contrast and phase contrast. Top: real world projection images of a thin sectioned articular cartilage specimen showing the impact of the distance between scintillator and sample on absorption contrast/ phase contrast (adapted from Zehbe[1] et al., 2009).

A promising methodology for certain imaging applications, where it is impossible to rely solely on absorption contrast, was introduced at third generation synchrotron sources (e.g.

ESRF, BESSY II or in the future PETRA III). This methodology requires a partially coherent beam and allows applying phase contrast to X-ray imaging techniques. While imaging in absorption contrast is well adapted to samples featuring a prominent difference in density or atomic mass, phase contrast imaging allows detection of structural details which are not well visible in absorption. Here, the contrast is achieved by retardation or refraction of coherent X-rays at phase boundaries inside the sample (Cloetens et al., 2006; Rack et al., 2008; Zehbe[1] et al., 2009). Fig. 2 illustrates the basic experimental setup which was used throughout this chapter and details the impact of the sample position relative to the scintillator on the resulting image contrast. The top left of Fig. 2 displays the projection images of a sliced bovine cartilage specimen mounted on a microscope slide being imaged at the same X-ray energy of 10 keV but different distances to the scintillator. Well visible is the increasing edge retrieval for the elliptical object with greater distance to the scintillator.

4. X-Ray Tomography and the Life Sciences

X-ray based tomography was first established by Hounsfield and Cormack (Hounsfield, 1973, Cormack, 1973) using an X-ray tube based setup. This work cumulated in the introduction of the first clinical X-ray tomography system in 1975. With the advancement of superior experimental setups new scientific applications became possible, allowing adapting tomographic experiments to much smaller samples while obtaining an unprecedented resolution on the micrometer scale. This methodology was consequently termed micro computed tomography (μCT).

One of the first medical related research fields in μCT was the analysis of trabecular bone samples by Feldkamp et al. (Feldkamp et al., 1989) but was soon extended to other areas including tissue engineering (Ho & Hutmacher, 2006). The superior properties of synchrotron generated X-rays further benefitted the tomographic analyses in the life sciences and became known as SR-μCT (Bonse & Bush, 1996). Finally, μCT (regardless of the origin of the X-ray) is heavily dependent on advanced computer technology benefiting significantly from the improvements in this field over the last 20 years. In this context, it should be noted that current tomographic data sets can easily amount to several hundred gigabytes in uncompressed size (e.g. approximately 280 Gigabytes for a data set of 4096 pixel x 4096 pixel x 4096 pixel in 32 bit grey values). Even nowadays the processing of such data can take a very long time or might even be impossible for single workstation computer systems. Concerning the experimental conditions, enhancements in scintillators (which are needed for the conversion of X-rays into visible light) and of course the high mechanical precision of modern rotational stages are prerequisites for acquiring high resolution tomographic data. In experiments which rely mainly on absorption contrast to image biological specimen, it is usually mandatory to significantly enhance this contrast. In this regard, metal staining commonly used in electron microscopy is a well adapted methodology especially if a discrimination of soft tissue structures is to be considered. One of the principal metal stains is osmiumtetroxide (OsO_4) which is a potent lipid stain and allows detection of cells or other lipid tissue structures. Using SR-μCT, OsO_4 has been used among many others by Ginty et al. to investigate cell seeded scaffolds (Ginty et al., 2006), by Lareida et al. to investigate the microstructure of the inner ear (Lareida et al., 2009) and by ourselves to detect cells inside a multilayered sheet scaffold as will be described later in section 7.4. A more specific staining can be achieved using immunhistochemical methods or

probes. In our own research (see section 7.1) we have established Au-lysine as a potent marker for anionic sites at the cell surface (Zehbe[2] et al., 2009).
To circumvent the usage of staining agents, which possibly introduce artefacts or which might occlude certain structural details from view, the application of phase contrast imaging is a valuable alternative. While a measurement in absorption contrast relies on the adaptation of the beam energy to the sample, phase contrast imaging relies solely on a coherent beam and therefore can be adjusted by varying the distance between sample and scintillator. In this measurement mode it is further possible to significantly reduce the dose applied to the sample by increasing the beam energy. In principle, this mode of operation allows imaging both strongly and weakly absorbing structures simultaneously. The reader is referred to the work of Cloetens et al. (Cloetens et al., 2006) and our own work (Zehbe[1] et al., 2009) for a more detailed discussion.

5. Tissue Engineering

In regenerative medicine, tissue engineering can be described as a tool to re-establish lost functionality and morphology to a previously damaged tissue. Over the years, several strategies were developed with combinations of cells and biomaterials playing a crucial role. These constructs are designed to be transplanted into the defect site and are already in clinical application. In orthopaedic surgery this methodology is usually termed matrix based autologeous chondrocyte transplantation. In this context, artificial scaffolds were introduced, allowing predefining a structure, into which cells can be expanded and immobilized *in vitro* or which serve as filler for migrating cells *in vivo*. Current tissue engineering strategies further adapt biochemical targeting to specifically stimulate proliferation, matrix synthesis or to control cell differentiation or cell migration. This last approach usually involves drug release concepts.
The archetype for all these tissue engineering strategies is the native and healthy tissue which should be regenerated and remodelled. From an investigational viewpoint, the gold standard defining this native structure is given by the analysis of histolochemically stained slices of the specimen. Unfortunately, this approach results in the complete loss of all volumetric morphological information, and requires complex procedures if it is to be recovered, usually involving alignment and registration of subsequent serial sections (Braverman et al., 1986). Due to its non destructive nature and its ability to resolve the true volumetric representation of a given specimen, μCT and especially SR-μCT have become important methods in the life sciences.
The following research details some possible applications in tissue engineering, putting a focus on cartilage tissue engineering. Later on, this chapter deals with approaches using stacks of polymer sheets for possible applications in neuronal tissue engineering.

6. Experimental Setup

Computed tomography (CT) requires a setup where either the sample or the beam source/ detector system (e.g. clinical CTs) are rotated relative to each other. For synchrotron radiation based experimental setups, a rotation of the beam source/ detector system is impossible. In this case, the sample is positioned on a multiaxial high precision rotational stage, allowing adjustment of translation, rotation and tilting. The experimental setup as

displayed in Fig.2 has been used predominantly in this chapter and is described in several studies (Zehbe[1] et al., 2007; Zehbe[1] et al., 2009; Rack et al., 2008). Although the photon flux density is several orders of magnitude higher than in X-ray tubes, it is not constant over the X-ray energy. Fig. 3 displays the dependency of the photon flux density from the X-ray energy as was calculated according to Schäffers et al. for the BAM*line* experimental station at BESSY II (Schäffers et al., 1996). Here, at around 10 keV, the photon flux density is dramatically reduced due to the used monochromator (DMM, see inset) being coated with tungsten (L3ab absorption edge at 10.198 keV). Accordingly, measurements in this energy range usually require longer exposure times due to the reduced photon flux when compared to for example measurements at around 22 keV. In the research detailed in this chapter, the energy was set to different values ranging from 7 keV to 30 keV, while further using different sample to scintillator distances as to achieving the desired contrast mode. The scintillator consisted of a thin, single $CdWO_4$ crystal and was coupled to light optics (up to 10x magnification) and a CCD camera (2048x2048, peltier cooled to -30 °C). The acquired projection images were recorded in multi-image file formats.

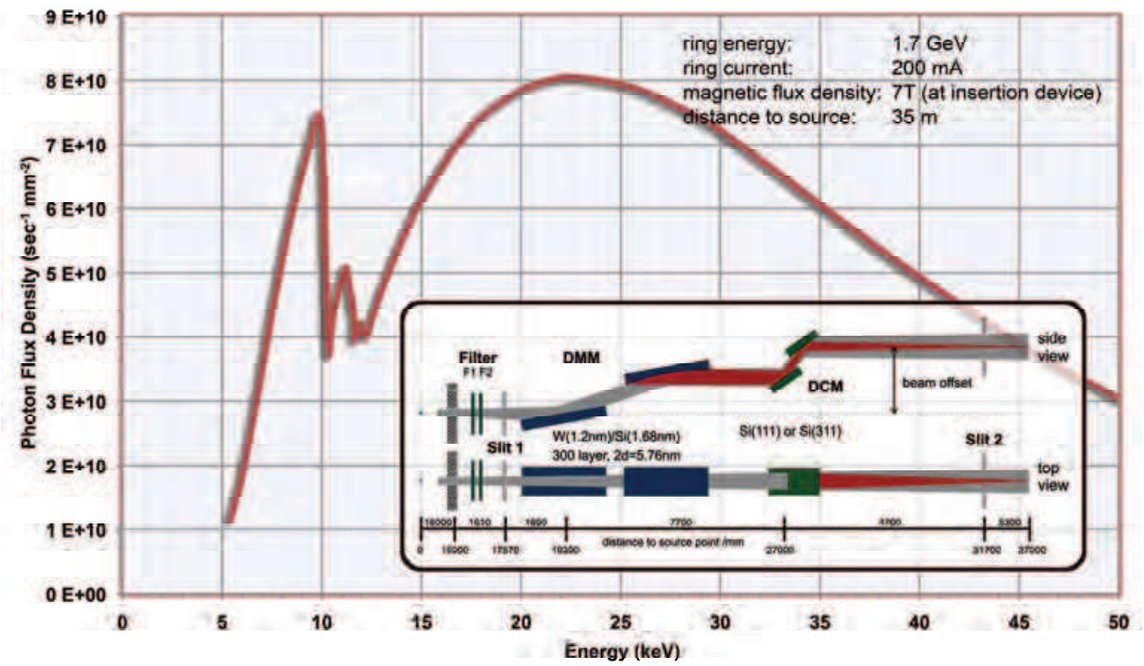

Fig. 3. Photon flux density behind the double multilayer monochromator (DMM) at the BAM*line* according to Schäffers et al. and Rack et al. (Schäffers et al., 1996, Rack et al., 2008). Around 10 keV the flux is reduced; data from BAM*line* description (Riesemeier et al. 2007).

7. Research

For an in-depth description of the experimental methodology and the results obtained, the reader is kindly referred to Table 2 at the end of this chapter and the cited references. Rendered data has been re-coloured for visualization purposes.

7.1 Cartilage Tissue Engineering

Degenerative, rheumatic or traumatic processes are the predominant causes for articular cartilage damage. The tissue itself has only a very limited regenerative potential and consequently, cartilage tissue engineering aims at either repopulating a defect with an excess amount of autologeous cells, stabilizing the defect area by supporting cell-scaffold constructs or enhancing the regeneration by biochemical targeting mechanisms. To better understand these different tissue engineering approaches it is mandatory to comprehend structure and function of the native tissue. Articular cartilage covers the ends of the long bones and is well known for its mechanical and tribological properties featuring a specific zonal structure of the extracellular matrix (primarily collagen II and proteoglycans) and the integrated cartilage cells, the chondrocytes. The following regions can be identified as follows: the surface zone, the middle zone, the deep zone and the subchondral bone (Buckwalter & Mankin, 1997). Depending on the zonal localisation, the chondrocytes appear in different morphologies. They are stretched along the surface as are the collagen fibres, while being mostly elliptical or rounded in the middle zone, where some cells form isogeneous cell groups. Towards the deep zone, the collagen fibres become more perpendicularly oriented to the surface resulting in a rise in stiffness. This zone further becomes increasingly calcified and connects to the subchondral bone.

In a previous study (Zehbe[1] et al., 2009) we have elucidated the use of SR-μCT to image the volumetric tissue morphology. Although the original data showed strong ring artefacts due to scintillator errors, as displayed in Fig. 4a, these artefacts were well compensated by sinogram correction as shown in Fig. 4b.

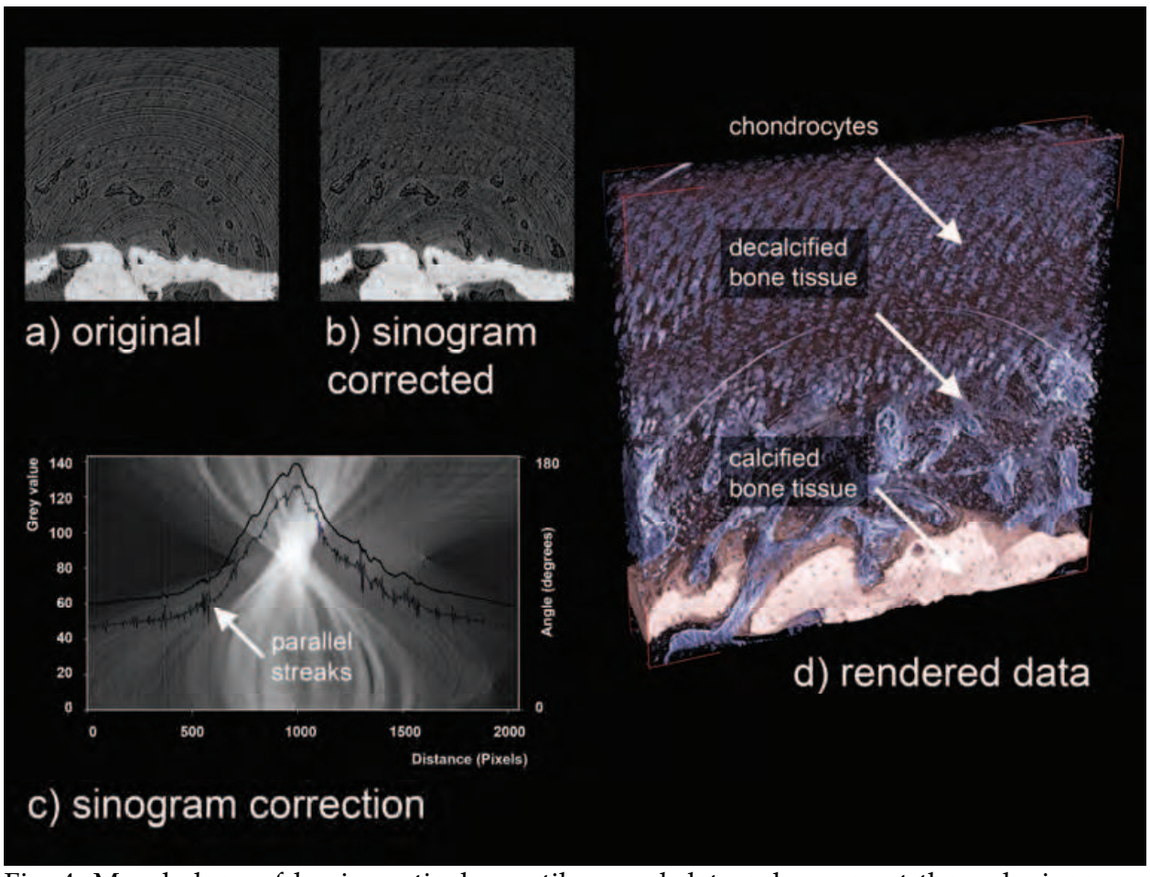

Fig. 4. Morphology of bovine articular cartilage and data enhancement through sinogram correction (a-c) resulting in the rendered data (d).

In the sinogram data (Fig. 4c), ring artefacts appear as parallel streaks or lines and can be easily filtered with a median filter. The data was rendered in a user defined colour scheme as displayed in Fig. 4d, showing the three-dimensional distribution and orientation of the chondrocytes depending on their zonal localisation.

Consequently, a tissue engineering approach should adapt as many of these properties as possible. As pure cell based tissue engineering can only partly re-establish the cellularity, usage of scaffold systems offers a methodology not only to restore the cellularity but also structure and function. These scaffolds are usually made of synthetic or natural polymers by techniques like fibre bonding, solvent casting, gas foaming or phase separation (Mikos & Temenoff, 2000). In our own research on scaffolds for cartilage tissue engineering, we developed a technique, which uses a directional freezing process to structure water based solutions of gelatine. This process was further designed to allow for the electrolysis of water prior to freezing and consequently results in the introduction of gas bubbles inside the gelatine solution before it is directionally frozen. Addition of other components like salts, acids, ceramics or polymer particles allows synthesising composite scaffolds or achieving different pore morphologies (Zehbe et al., 2005; Zehbe[1] et al., 2007; Zehbe[2] et al., 2009).

Fig. 5 displays some rendered representations of scaffolds made by ourselves and which are designed to degrade biologically.

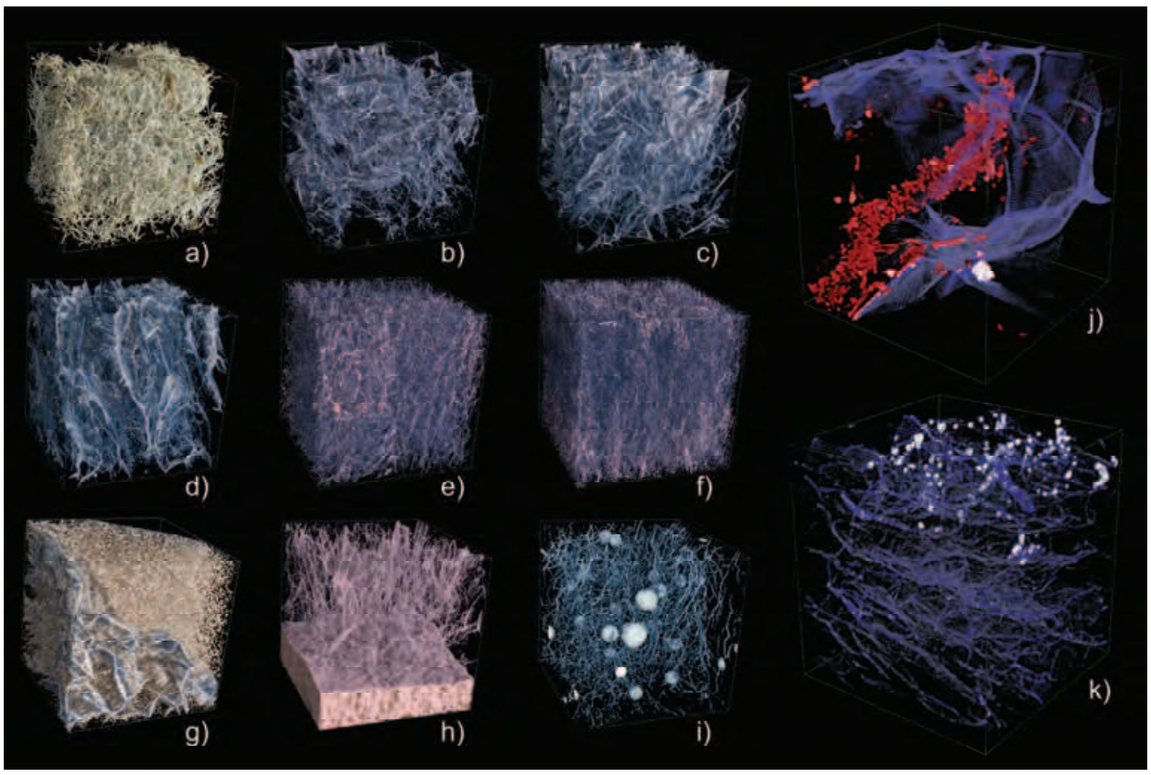

Fig. 5. Scaffolds for cartilage tissue engineering. a) Ethisorb ®, b) – f) gelatine scaffolds with increasing pore diameter, g) gelatine scaffolds with cells in fibrin matrix, h) gelatine-hydroxyapatite-composite scaffolds, i) PLGA-microsphere modified gelatine scaffold, j) scaffold with manual separated cells (red) and Au/ Ag stained cells (white) and k) scaffold with Au/ Ag stained cells (white) at the surface only.

Fig. 5a shows a competing commercial type scaffold (Ethisorb ®) which is made of PLGA-fibres being connected by poly-p-dioxanone and which was cultivated with porcine chondrocytes (2 * 10^6 cells) for 1 week, although the SR-µCT data did not reveal cells, the scaffold morphology was well imaged.
Figs. 5b to 5f demonstrate the effects of different freezing temperatures and differing ion contents (here, addition of hydrochloric acid) on the pore morphology as outlined in Table 1. The Feret's diameter of the pores was calculated as mean value from each slice of the respective tomographic data (Zehbe[2] et al., 2009). All these gelatine scaffolds were cultivated with porcine chondrocytes similar to the commercial Ethisorb® scaffold as described above. Further, the cultivated cells were labelled with a cell surface specific metal stain (Au-lysine in combination with a silver enhancer) to better visualize individual cells in the tomographic data.

Scaffold (as labelled in Fig. 5)	b)	c)	d)	e)	f)	j)	k)
Freezing temperature (°C)	-10	-10	-10	-20	-30	*-10*	*-20*
HCl content (1 molar) (ml/ml)	0.08	0.04	0.00	0.00	0.00	*0.08*	*0.00*
Pore diameter (Feret) (µm)	606	374	240	131	67	*606*	*131*

Table 1. Parameters influencing the pore morphology of gelatine scaffolds (scaffold b) and j) and scaffold e) and k) are identical).

Interestingly, this staining did not label all cells as intensely as desired (Fig. 5j). Consequently, cells were individually separated using a software-based volumetric mark-up tool. As a result, it was only possible to demonstrate a homogeneous and dense population of cells inside the larger pored scaffolds (Fig. 5b/ 5j), while the denser scaffolds appeared to show intensely stained cell-clusters at the surface only (Fig. 5e/ 5k).
In a different approach we infiltrated scaffolds with a cell-suspension containing fibrin to immobilize the cells immediately after seeding inside the scaffold. This approach was partly successful, as it allowed for a better seeding efficacy but resulted in a layer of fibrin and cells at the surface of the scaffold only (Fig. 5g). Due to the increased phase contrast in this SR-µCT experiment, it was possible to identify individual cells rather easily (cells can be seen as grainy structure on top of the scaffold).
Another two completely different gelatine scaffolds were made by incorporating hydroxyapatite (HAp) as a bottom layer being designed to seal against the subchondral bone *in vivo* (Fig. 5h) and by distributing polymeric poly-lactide-co-glycolide (PLGA) microspheres inside the gelatine suspension (Fig. 5i). These microspheres were intended as possible carriers for targeting molecules (here: prostaglandine E_2, PGE_2) in a drug-release setup. The morphology and the design of the drug-loaded PLGA-microspheres are further detailed in section 7.3. From a tomographic viewpoint these different components were easily separated from the gelatine network, revealing their respective structures rather well. Due to all components having differing elemental compositions or densities, imaging was performed in absorption contrast (Zehbe[1] et al., 2007).
On the other hand absorption contrast cannot be well utilized for scaffolds in a watery or swollen state. Consequently, further experiments were conducted using phase contrast imaging to elucidate the resistance of the scaffolds against compression in a wet environment as detailed in the following section.

7.2 Mechanics and Morphology of Scaffolds for Cartilage Tissue Engineering

Articular cartilage demonstrates mechanical and tribological properties allowing lifelong relative movement of adjacent bones. Tissue engineering concepts, especially those dealing with artificial scaffolds, should, if possible, adapt these properties to some extend.
In this regard, an early study of us (Zehbe et al., 2004) proved near native mechanical properties for gelatine scaffolds with a highly directional pore structure as discussed in the previous section. Mechanical testing of the water soaked scaffolds in confined and unconfined conditions showed a strain increase caused by fluid efflux, typical for biphasic

materials. Young's moduli were determined to E_s = 0.67 ± 0.02 MPa in unconfined compression, aggregate moduli to H_A = 0.84 ± 0.03 MPa in confined compression and the Poisson's ratio to ε_s = 0.27. The obtained values correspond well with bovine cartilage tissue measured by Korhonen et al. (Korhonen et al., 2002).
Until now, we were not able to determine the three-dimensional structural changes of these scaffolds under mechanical load. Therefore, we adapted SR-µCT in phase contrast imaging mode to determine structural changes, while completely immersing the scaffolds in water.

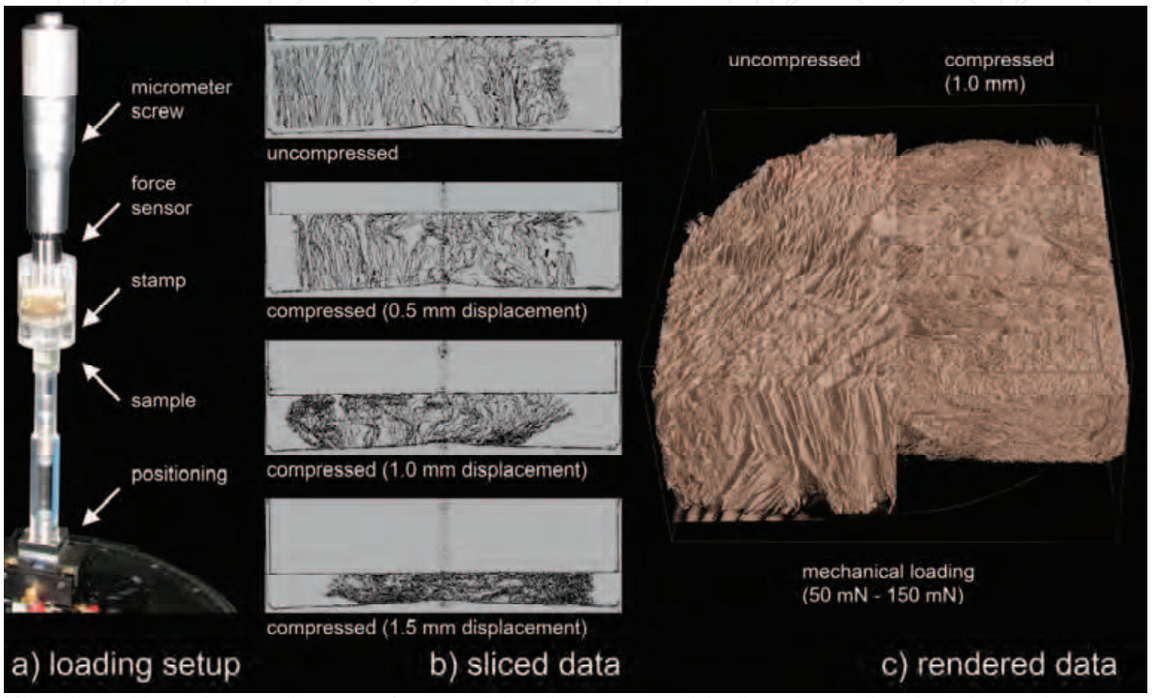

Fig. 6. a) Experimental setup for combined tomographical and mechanical investigations, b) acquired sliced data of subsequent mechanical displacements and c) rendered data comparing two different compression levels.

Although the absorption coefficients for water and gelatine are almost similar and would make it extremely difficult to achieve any tomographic details in absorption, phase contrast imaging in this case allows for an excellent contrast. Consequently, we have established an experimental setup (Fig. 6a) allowing simultaneous mechanical loading and tomographic measurement of water soaked gelatine scaffolds. The loading setup consisting of a micrometer screw, a plexiglas rod and a simple force sensor is described in more detail in Thiem et al. (Thiem et al., 2009). Briefly, a water soaked and air bubble free scaffold was placed inside the plexiglas rod while carefully adjusting the on top stamp and calibrating the force sensor. This whole setup was placed on the sample stage and was adjusted in the beam. The maximum possible distance of 109 cm between sample and scintillator and a beam energy of 30 keV ensured sufficient phase contrast to detect the scaffold structure in the watery environment as seen in the sliced data (Fig. 6b) and in the rendered data (Fig. 6c). The parallel pore network appears to bulge at specific sites (Fig. 6b – 1.0 mm displacement) upon increasing the load. As a result most of the mechanical energy is dissipated at these sites, while leaving the overall scaffold structure mostly intact. Upon further loading, the

pore network cannot withstand and the pore channels collapse (Fig. 6b – 1.5 mm displacement). Summarizing the previously measured biphasic material properties and the newly acquired three-dimensional morphological data, we expect good mechanical properties *in vivo* as well.

7.3 Polymeric Drug Release System for Cartilage Tissue Engineering

Current tissue engineering concepts consider biomolecular targeting mechanisms aimed at specific cells the most feasible approach towards successful tissue regeneration. Consequently, the integration of targeting molecules into scaffold materials might significantly improve the quality and long-term performance of the regenerating tissue by maintaining cellular differentiation and optimal tissue functions. In this context, numerous substances are known to promote tissue regeneration by stimulation of specific cellular pathways. Well established in bone and cartilage tissue engineering are the members of the TGF-β superfamily, including the bone morphogenic proteins (BMP) and other related substances (Nicoll et al., 1998).

From the viewpoint of cartilage tissue engineering another promising class of targeting molecules has been found in the metabolites of the arachidonic acid – namely prostaglandine E_2, which has been demonstrated being important in both developmental processes and in tissue regeneration (Sandulache et al., 2006) including bone repair and cartilage regeneration. One limiting factor which applies to many targeting molecules is their short half-life *in vivo*. One possibility to prolong the availability *in vitro* or *in vivo* is to encapsulate the targeting molecule directly inside the scaffold material or indirectly by using a more defined carrier system like polymeric microspheres.

In previous studies we have adapted this later approach and were able to successfully encapsulate PGE_2 into polymeric polylactide-co-glycolide microspheres (Watzer et al., 2009). For more detailed information, the reader is referred to the chapter by Brochhausen et al. in this same book. The integration of these microspheres into a gelatine scaffold was briefly described in section 7.1. Unfortunately, the data obtained by SR-μCT did not reveal ultrastructural details, probably due to a too low difference in absorption contrast, which was the dominant image contrast. A reinvestigation (Zehbe[3] et al., 2009) of single microspheres at a slightly higher resolution but in phase contrast imaging mode revealed the data presented in Fig. 7. Apparently, the PGE_2-loaded PLGA-microspheres feature a porous shell with a compact core (Fig. 7a and Fig. 7c). It is currently unknown if this porosity is due to local solvent-entrapment and accumulation, while the PLGA continuously hardens, forming hollow structures or, some other mechanism.

This structural data might explain the release profile (Brochhausen et al., 2008), which is shown in Fig. 7b, showing a burst release early on with a plateau after 24 h and decreasing release afterwards. The more porous shell can probably release the PGE_2 much faster than the compact core which functions as diffusion barrier limiting the progress of the target molecule from the inside to the outside.

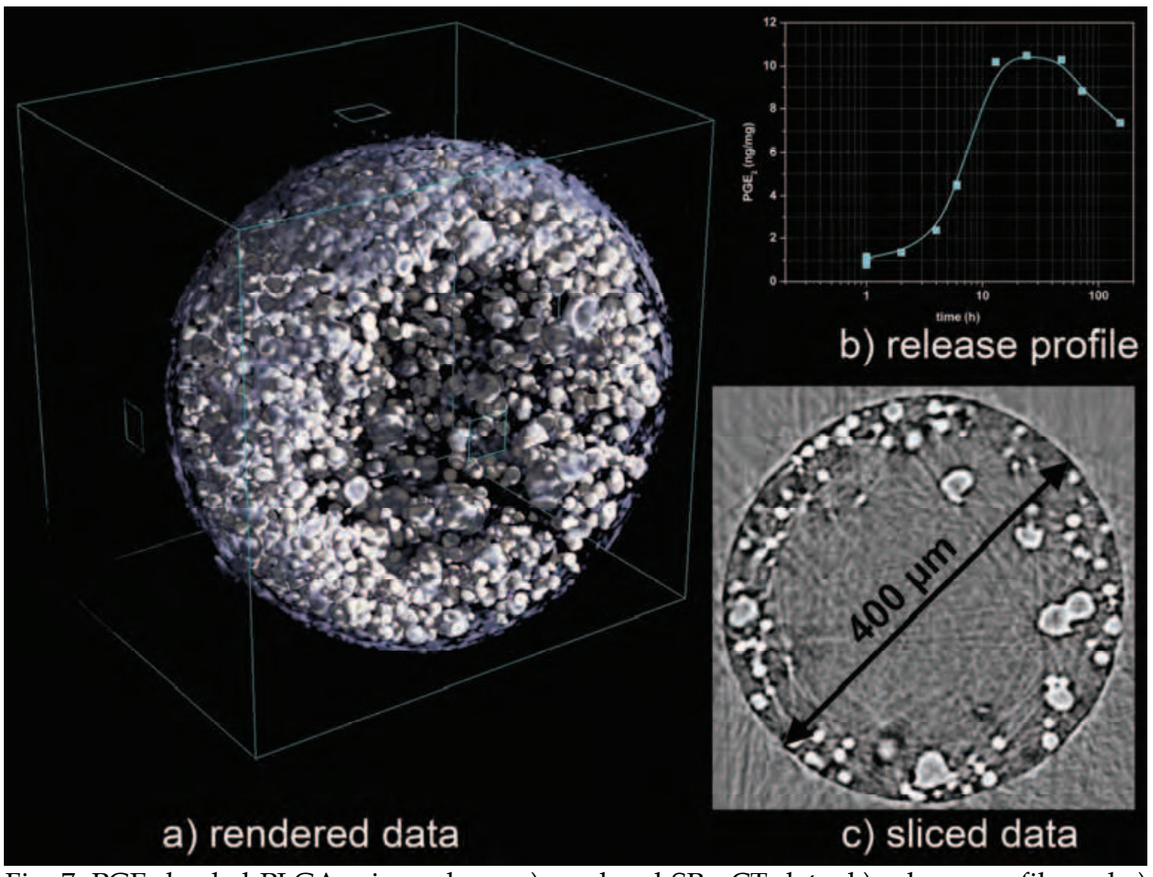

Fig. 7. PGE_2-loaded PLGA microsphere: a) rendered SR-µCT data, b) release profile and c) sliced SR-µCT data.

7.4 A Different Type of Cell Sheet Engineering investigated by SR-µCT

A few years ago a novel cell culture technology was developed and termed *cell sheet engineering* (Shimizu et al., 2003). This technology uses a thermoresponsive polymer (poly(N-isopropylacrylamide, PIPAAm) to detach cultivated monolayer cells from tissue culture ware by changing the PIPAAm from a hydrophilic state to a hydrophobic state by decreasing the temperature below 32 °C. The main advantage of this technology is that a pure (autologeous) cell sheet can be harvested without any supporting biomaterial which can be beneficial in applications, where an artificial material is not desired. Further, these cell sheets can be stacked. Due to the monolayer nature of this tissue engineering technique, only relatively thin cell layer aggregates can be achieved. To achieve a thicker more scaffold like structure, we have developed a different approach by cultivating cells on thin composite coatings of PLGA and gelatine on cell culture ware. As the gelatine gradually swells in cell culture and partly dissolves, the resulting porous PLGA-gelatine sheet and the cells on top can be easily detached from the cell culture ware either for further *in vitro* experimentation or by stacking these sheets obtaining a layered structure of cells and supporting biomaterial.

Fig. 8 displays a stack of 13 PLGA-gelatine sheets which were cultivated with a chondrocyte cell line (CHON-001) and which were afterwards fixated using glutaraldehyde and stained

with OsO_4. Due to the enhanced absorption contrast resulting from using OsO_4 a morphological differentiation between cells and supporting PLGA-gelatine-sheets can be achieved via SR-µCT.

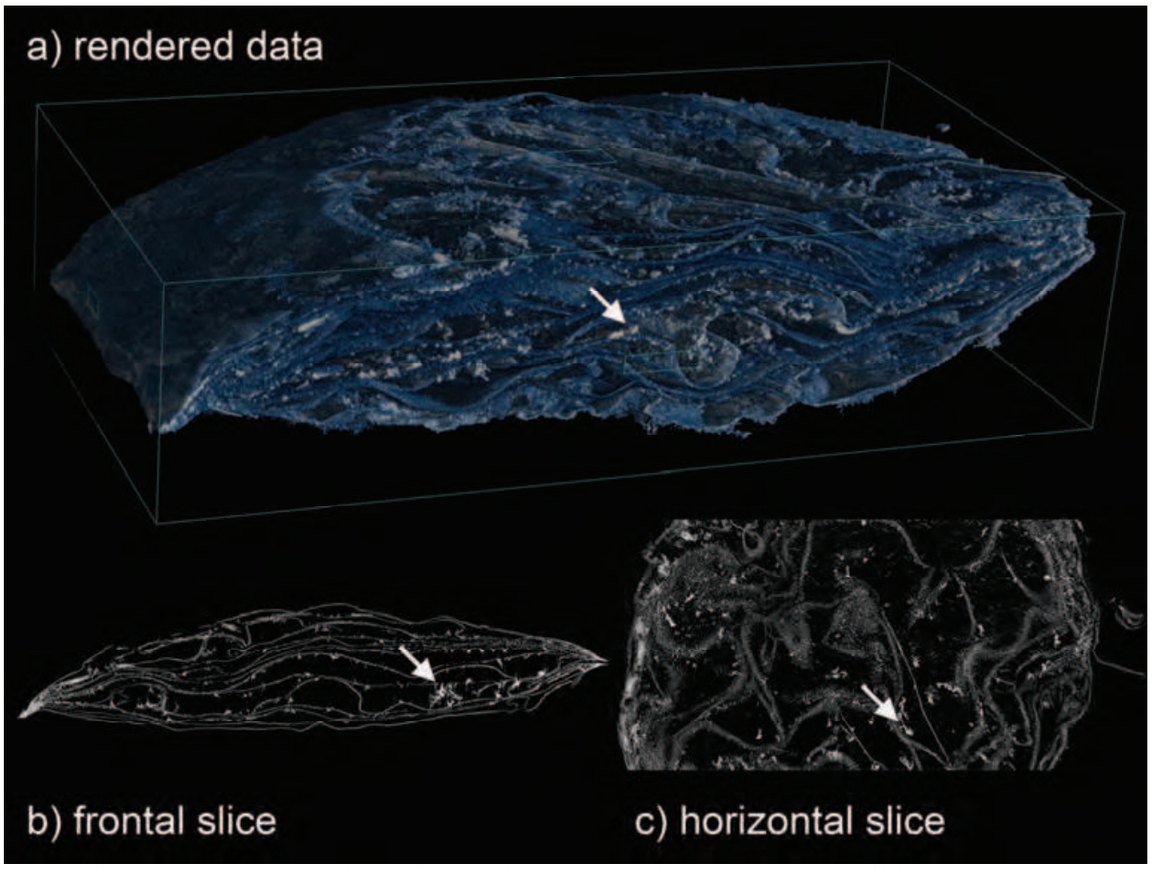

Fig. 8. Stack of thirteen PLGA-gelatine sheets pre-cultivated with a cell line, glutaraldehyde fixated and OsO_4 stained. a) rendered data, b) and c) sliced data (frontal and horizontal).

While Fig. 8a displays the rendered SR-µCT data, Figure 8b and 8c display the corresponding frontal and horizontal sliced data. Arrows indicate exemplarily locations of OsO_4 stained cells, which exhibit a strong absorption contrast sometimes resulting in artefacts due to shading effects. Overall, the structural data obtained indicates possible applications in the area of the tissue engineering of articular cartilage, skin or nerve tissue. Further, nerve tissue engineering is the topic of the following section describing yet another approach using stacked polymer sheets.

7.5 Neuronal Tissue Engineering

Restoring peripheral nerve damage is an important research field in tissue engineering sciences. One promising approach uses so called nerve conduits consisting of biodegradable polymers. The intention for using these conduits is to establish a preformed structure serving as guidance for axonal growth *in vivo*.

In this context, it can be beneficial to prearrange autologeous neuronal cells inside these conduits to achieve a better control over axonal growth e.g. by structural, biochemical or physical means. Biochemical stimulation can be achieved by integrating certain targeting molecules into the conduits similar to the methodology described in section 7.3. Here, the nerve growth factor protein (NGF) is probably the most relevant biochemical substance in neuronal tissue engineering (Bhang et al., 2007). Its usage is one of several other biochemical and physical mechanisms that can be applied to control neuronal regeneration (Schmidt[1] et al., 2009). Concerning physical stimulation, it is well known, that neuronal cells are especially susceptible to electrical potentials. Therefore, in the following research, we present a rather simple methodology to control cell growth by applying an electrical potential and we demonstrate that SR-µCT can be used to confirm the efficacy from a three-dimensional morphological viewpoint (Schmidt[2] et al., 2009).

One major problem occurring in tissue engineering can be attributed to the fact that cells usually grow in a non ordered fashion *in vitro*. Consequently, we have developed a technique to print microelectrodes on polymer sheets via a method named *inverse ink-jet printing* (using a sputter coater to establish a gold metallization) allowing for vital co-deposition of cells and the protein fibrin on the anode part of the electrodes (Zehbe[2] et al. 2007). While the structural resolution of the electrodes is limited by the used printer, a minimal line width of 35 µm was achievable with a HP deskjet 3520. At first, this method was designed for two-dimensional cell cultivation purposes, but was later extended into the third dimension by stacking - similar to section 7.4.

The electrodes being designed for an intended use in neuronal tissue engineering feature parallel aligned rows of thin gold made by the sputter coating process. All rows were contacted anodically allowing for deposition of cells and fibrin. Afterwards, several microelectrodes with the on top cells were stacked, fixated using glutaraldehyde, rinsed in distilled water and freeze-dried for further SR-µCT investigations. One microelectrode was used for separate vital staining using fluoresceindiacetate/ ethidiumbromide and displays nearly 100% vitality (see Fig. 9c). Moreover, the cells were found to adhere solely on the anode parts of the electrodes – an effect which we think results from the co-deposited fibrin network, serving as artificial extracellular matrix immobilizing the deposited cells.

Concerning the following SR-µCT imaging experiments, the final imaging results were rather interesting and unexpected. As the experiments were conducted in absorption contrast only, the expected result would have been to observe strongly absorbing deposited gold structures and a weekly absorbing polymer substrate. Further, as the deposited cells were not stained with any metal stain (like OsO_4), we did not expect to observe the cells themselves, as they have a low density and are thin compared to the polymer substrate.

But interestingly, cells were imaged well (Fig. 9a and 9b) and in good accordance with the fluorescence microscopic images acquired previously. This effect is even more astonishingly, as the cells appear as even stronger absorbing structures than the deposited gold layer. Currently, we do not have a valid explanation for this imaging result.

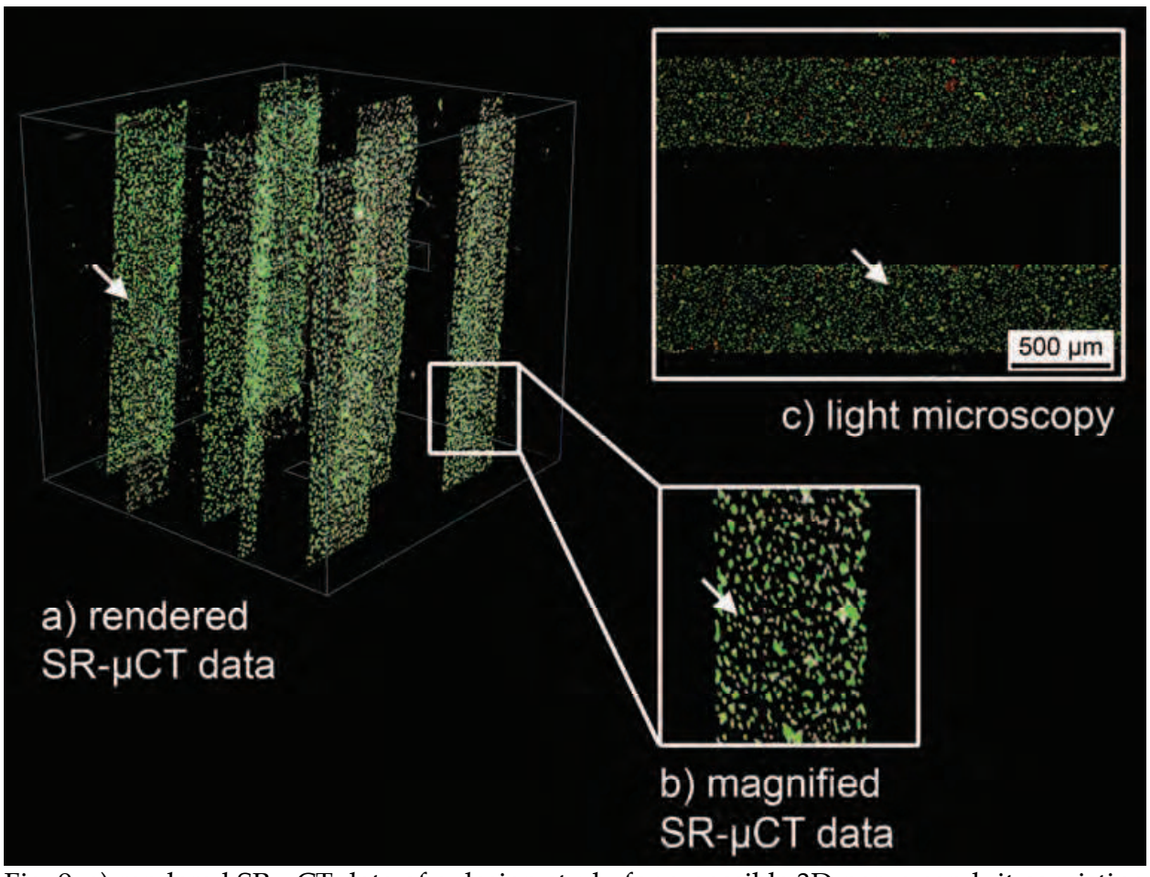

Fig. 9. a) rendered SR-µCT data of a design study for a possible 3D-nerve conduit consisting of stacked micro electrodes, b) magnified SR-µCT data showing single cells and c) corresponding fluorescence microscopic image of a vital stain showing 100 % vital cells.

8. Discussion and Conclusion

In this chapter we have given a brief overview of some tissue engineering strategies and biomaterials concepts while focussing on high resolution SR-µCT imaging.

As was stated previously the presented research should be viewed in the light of the respective references, which give more detailed information. Among the described tissue engineering solutions, the most extensive research has been conducted on gelatine scaffolds with an adjustable pore network for articular cartilage tissue engineering. These scaffolds were designed to allow for further optimizations by introducing other substances like hydroxyapatite as filler for subchondral bone defects or by addition of biochemical targeting molecules to stimulate tissue regeneration. Here, prostaglandine E_2 was immobilized exemplarily in polylactide-co-glycolide microspheres for extended release, while distributing the microspheres in the pore structure of the gelatine scaffolds.

The presented tomographic data for this tissue engineering solution detailed both cells and scaffold materials down to a voxel resolution of 1.6 µm.

One major advantage of synchrotron radiation based µCT in combination with a highly coherent beam was found in the enhanced phase contrast imaging capabilities of the used

beamline in some experiments. Here, the demonstration of the pore channel collapse under mechanical loading resolved structures otherwise not visible in absorption contrast.
A resolution up to single biological cells was demonstrated in different imaging conditions. While OsO_4 and a combination of Au-lysine with a silver enhancer were used to increase the imaging results in absorption contrast, phase contrast imaging was adapted to image individual cells in both native cartilage tissue and inside gelatine scaffolds as well. A rather interesting result was found for a stack of microelectrodes, where exceptionally well resolved single cells were found in absorption contrast.
In conclusion, SR-μCT is a promising methodology to investigate tissues or tissue engineered biomaterial-cell constructs. Due to the superior photon quality generated in modern synchrotron facilities a far more adaptable setup is established to solve specific scientific problems, otherwise not possible in X-ray tube μCT experimental setups. For example, this technique opens up the possibilities for *in situ* measurements of living tissues e.g. mechanical loading experiments, acquiring time-lapse tomographic data.

9. Acknowledgments

This study was supported partly by the Deutsche Forschungsgemeinschaft (DFG) by grants SCHU 679/27-1 & SCHU 679/27-2.
The authors would like to thank U. Gross, A. Thiem, B. Watzer, R. Grupp and M. Dilger for discussions and technical assistance.

10. References

Bernhardt, R.; Scharnweber, D.; Müller, B.; Thurner, P.; Schliephake, H.; Wyss, P.; Beckmann, F.; Goebbels, J. & Worch, H. (2004). Comparison of microfocus- and synchrotron X-ray tomography for the analysis of osteointegration around Ti6Al4V implants, *European cells & materials*, 7, 42-51

Bhang, S.H.; Jeon, O.; Choi, C.Y.; Kwon, Y.H. & Kim, B.S. (2007). Controlled release of nerve growth factor from fibrin gel, *J Biomed Mater Res A*, 80, 998-1002

Bonse, U. & Busch, F. (1996). X-ray computed microtomography (μCT) using synchrotron radiation (SR), *Prog. Biophys. molec. Biol.*, 65, 1-2, 133-169

Braverman, M.S. & Braverman, I.M. (1986). Three-dimensional reconstructions of objects from serial sections using a microcomputer graphics system, *J. Invest. Dermatol.*, 86, 290–294

Brochhausen, C.; Zehbe, R.; Watzer, B.; Halstenberg, S.; Gabler, F.; Schubert, H. & Kirkpatrick, C.J. (2008), Immobilization and controlled release of prostaglandin E_2 from poly-L-lactide-co-glycolide microspheres, *J Biomed Mat Res A*, published online, DOI: 10.1002/jbm.a.32215

Buckwalter, J.A. & Mankin, H.J. (1997). Articular Cartilage, Part I: Tissue Design and Chondrocyte-Matrix Interactions, *Journal of Bone and Joint Surgery*, 79A, 600-611

Cloetens, P.; Mache, R.; Schlenker, M. & Lerbs-Mache, S. (2006). Quantitative phase tomography of Arabidopsis seeds reveals intercellular void network, *PNAS*, 103, 39, 14626-14630

Cormack, A.M. (1073). Reconstruction of densities from their projections, with applications in radiological physics, *Physics in Medicine and Biology*, 18, 195-207

Dilmanian, F.A. (1992). Computed tomography with monochromatic X-rays, *American journal of physiologic imaging*, 7, 3-4, 175-93

Feldkamp, L.A.; Goldstein, S.A.; Parfitt, A.M.; Jesion, G. & Kleerekope, M. (1989). The direct examination of three-dimensional bone architecture *in vitro* by computed tomography, *J Bone Min Res*, 4, 3-11

Ginty, P.J.; Howard, D.; Rose, F.R.A.J.; Whitaker, M.J.; Barry, J.J.A.; Tighe, P.; Mutch, S.R.; Serhatkulu, G.; Oreffo, R.O.C.; Howdle, S.M. & Shakesheff, K.M. (2006). Mammalian cell survival and processing in supercritical CO_2, *PNAS*, 103, 19, 7426-7431

Ho, S.T. & Hutmacher D.W. (2006). A comparison of micro CT with other techniques used in the characterization of scaffolds, *Biomaterials*, 27, 1362–1376

Hounsfield, G.N. (1973). Computerized transverse axial scanning (tomography). Part I: Description of system. Part II: Clinical applications, *British Journal of Radiology*, 46, 1016-1022

Kak, A. & Slaney M. (1988). *Principles of Computerized Tomographic Imaging*, IEEE Press, New York

Korhonen, R.K.; Laasanen, M.S.; Töyräs, J.; Rieppo, J.; Hirvonen, J.; Helminen, H.J. & Jurvelin, J.S. (2002). Comparison of the equilibrium response of articular cartilage in unconfined compression, confined compression and indentation, *Journal of Biomechanics*, 35, 903-909

Mikos, A. & Temenoff, J. (2000). Formation of highly porous biodegradable scaffolds for tissue engineering, *Electronic Journal of Biotechnology*, 3, 2, 1-6

Nicoll, S.B.; Denker, A.E. & Tuan, R.S. (1998). Mesenchymal cell-based repair of connective tissue defects: Application of transforming growth factor-b superfamily members and biodegradable polymer scaffolds, *Cell Mater*, 8, 99–122

Rack, A.; Zabler, S.; Müller, B.R.; Riesemeier, H.; Weidemann, G.; Lange, A.; Goebbels, J.; Hentschel, M. & Görner, W. (2008). High resolution synchrotron-based radiography and tomography using hard X-rays at the BAM*line* (BESSY II). *Nuclear Instruments and Methods in Physics Research A*, 586, 327-344

Riesemeier, H.; Müller, B.R.; Radtke, M. (2007). BAM*line* Description (ID-02-2, 7T-WLS-BAMline, October 2007), http://www.bessy.de/upload/bitpdfs/ID_02_2.pdf

Röntgen, W.C. (1895). On a New Kind of Rays, *Nature,* 53, 274-276

Sandulache, V.C.; Parekh, A.; Li-Korotky, H.S.; Dohar, J.E. & Hebda, P.A. (2006). PGE_2 differentially modulates human fetal and adult dermal fibroblast migration and contraction: implication for wound healing, *Wound Rep Reg*, 14, 633-643

Schäfers, F. & Krumrey, M. (1996). REFLEC, Program to calculate VUV/ X-ray optical elements and synchrotron radiation beamlines, *BESSY, TB 201/96*

Schmidt[1], F.; Ghalanbor, Z.; Thormann, F.; Kühbacher, M.; Gross, U.; Bodmeier, R.; Schubert, H. & Zehbe, R. (2009). Drug Loaded, Biodegradable Nerve Conduits For The Simultaneous Chemical And Electrical Stimulation Of Neural Cells As A Therapeutic Approach For Peripheral Nerve Regeneration, *Materials Science Forum/ Advanced Materials Research*, Trans Tech Publications, accepted

Schmidt[2], F.; Kühbacher, M.; Gross, U.; Kyriakopoulos, A.; Schubert, H. & Zehbe, R. (2009). From 2D Slices to 3D Volumes: Characterization of Neuronal Cells Deposited on Anodic, Cationic and Uncharged Surfaces Using Dual Beam SEM/ FIB Serial Sectioning, submitted to *Ultramicroscopy*

Shimizu, T.; Yamato, M.; Kikuchi, A. & Okano, T. (2003). Cell sheet engineering for myocardial tissue reconstruction, *Biomaterials*, 24, 13, 2309-2316

Thiem, A.; Lum, V.; Grupp, R.; Riesemeier, H.; Bordia, R.; Schubert, H. & Zehbe, R. (2009). Synchrotron µCT Investigation of the Collapsing Pore-Network of Gelatin Scaffolds under Compression, *Materials Science Forum/ Advanced Materials Research*, Trans Tech Publications, accepted

Watzer, B.; Zehbe, R.; Halstenberg, S.; Kirkpatrick, C.J. & Brochhausen, C. (2009). Stability of prostaglandin E_2 (PGE_2) embedded in poly-D,L-lactide-co-glycolide microspheres - a pre-conditioning approach for tissue engineering applications, *J Mater Sci: Mater Med*, 20, 1357-1365

Zehbe, R.; Gross, U. & Schubert, H. (2004). Oriented collagenbased/hydroxyapatite matrices for articular cartilage replacement, *Key Engineering Materials*, 254-256, 1083-1086

Zehbe, R.; Libera, J.; Gross, U. & Schubert, H. (2005). Short-term human chondrocyte oriented collagen coated gelatine for cartilage replacement, *Bio-Medical Materials and Engineering*, 15, 445–454

Zehbe[1], R.; Haibel, A.; Brochhausen, C.; Gross, U.; Kirkpatrick, C.J. & Schubert, H. (2007). Characterization of oriented protein-ceramic and protein-polymer-composites for cartilage tissue engineering using synchrotron µ-CT, *Int J Mat Res*, 98, 562-568

Zehbe[2], R.; Gross, U.; Knabe, C.; Radlanski, R.J. & Schubert, H. (2007). Anodic cell-protein deposition on inverse inkjet printed micro structured gold surfaces, *Biosensors & Bioelectronics*, 22, 1493-1500

Zehbe[1], R.; Haibel, A.; Riesemeier, H.; Gross, U.; Kirkpatrick, C.J.; Schubert, H.; Brochhausen, C. (2009). Going beyond Histology: Synchrotron µCT as a Complementary Methodology for Biological Tissue Characterization, *Journal of the Royal Society: Interface*, published online: DOI: 10.1098/rsif.2008.0539

Zehbe[2], R.; Goebbels, J.; Ibold, Y.; Gross, U. & Schubert, H. (2009). Investigation of the Spatial Distribution of *in vitro* Cultivated Chondrocytes in Gelatine Scaffolds with varying Porosities – a Tomographic Approach, submitted to *Acta Biomaterialia*

Zehbe[3], R.; Watzer, B.; Grupp, R.; Halstenberg, S.; Riesemeier, H.; Kirkpatrick, C.J.; Schubert, H. & Brochhausen, C. (2009). Tomographic and Topographic Investigation of Poly-D,L-Lactide-Co-Glycolide Microspheres Loaded with Prostaglandin E_2 for Extended Drugrelease Applications, *Materials Science Forum/ Advanced Materials Research*, Trans Tech Publications, accepted

Section	Sample	Sample preparation	SR-μCT parameters *)					Reference
			Contrast mode	D_{ss} (cm)	E (keV)	t_e (s)	s_v (μm)	
7.1	bovine joint cartilage	aldehyde fixation, EDTA treatment, and ethanol dehydration	Phase	15	14	2.0	~1.6	Zehbe[1] et al., 2009
7.1	commercial scaffold (Ethisorb)	Seeded and cultivated with chondrocytes for 1 week. Following, aldehyde fixation and Au/Ag-staining, followed by rapid freezing and freeze-drying.	Absorption	<1.5	10	0.5	~3.7	-
7.1	gelatine scaffolds (according to Figs. 5b – 5f)	The pore morphology was modified during synthesis by varying the freezing temperature (d, e, f) and the ion content (b, c, d). Further sample treatment identical to Ethisorb scaffold	Absorption	<1.5	10	0.5 - 1.0	~3.7	Zehbe[2] et al., 2009
7.1	gelatine-fibrin composite scaffold	Similar to scaffold d) but infiltrated with cells suspended in fibrin glue.	Phase	60	20	1.5	~2.1	-
7.1	gelatine-HAp-composite scaffold	Deposition of hydroxyapatite (HAp) as bottom layer by sedimentation.	Absorption	<1.5	15	0.7	~3.6	Zehbe[1] et al., 2007
7.1	PLGA-microsphere gelatine scaffold	Inclusion of PLGA-microspheres into scaffold by suspension/ gelling	Absorption	<1.5	10	1.2	~3.6	Zehbe[1] et al., 2007
7.2	mech. loaded gelatine scaffolds	Samples measured in wet condition inside a loading apparatus.	Phase	109	30	0.7 - 0.8	~4.3	Thiem 2009
7.3	PGE_2 loaded PLGA-microsphere	Drug loaded microsphere, synthesized via emulsion.	Phase	30	20	1.8	~2.1	Zehbe[3] et al., 2009
7.4	PLGA-gelatine-multilayer	Layer of 13 PLGA-Gelatine sheets (40 % PLGA, 60 % Gelatine) cultivated with CHON-001 cells and OsO_4 stained.	Absorption	1.5	7	5.5	~2.1	-
7.5	microelectrode multilayer	Layer of 4 microelectrodes cultivated with fibroblasts	Absorption	<1.5	10	0.6	~3.6	Schmidt[1] et al., 2009

Table 2. Condensed experimental data for all samples in this chapter (for a detailed description, the reader is referred to the corresponding section and the cited references).

*) D_{ss}: Distance between sample and scintillator, E: X-ray energy, t_e: exposure time, s_v: voxel-size

IntechOpen

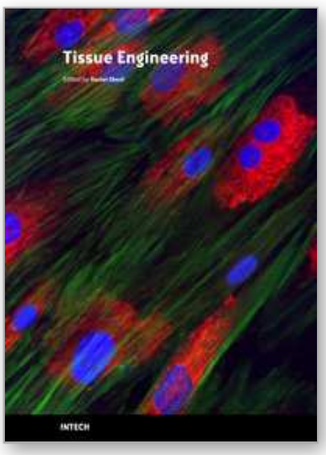

Tissue Engineering

Edited by Daniel Eberli

ISBN 978-953-307-079-7
Hard cover, 524 pages
Publisher InTech
Published online 01, March, 2010
Published in print edition March, 2010

The Tissue Engineering approach has major advantages over traditional organ transplantation and circumvents the problem of organ shortage. Tissues that closely match the patient's needs can be reconstructed from readily available biopsies and subsequently be implanted with minimal or no immunogenicity. This eventually conquers several limitations encountered in tissue transplantation approaches. This book serves as a good starting point for anyone interested in the application of Tissue Engineering. It offers a colorful mix of topics, which explain the obstacles and possible solutions for TE applications.

How to reference

In order to correctly reference this scholarly work, feel free to copy and paste the following:

Zehbe Rolf, Haibel Astrid, Schmidt Franziska, Riesemeier Heinrich, Kirkpatrick C. James, Schubert Helmut and Brochhausen Christoph (2010). High Resolution X-Ray Tomography - 3D Imaging for Tissue Engineering Applications, Tissue Engineering, Daniel Eberli (Ed.), ISBN: 978-953-307-079-7, InTech, Available from: http://www.intechopen.com/books/tissue-engineering/high-resolution-x-ray-tomography-3d-imaging-for-tissue-engineering-applications

INTECH
open science | open minds

InTech Europe
University Campus STeP Ri
Slavka Krautzeka 83/A
51000 Rijeka, Croatia
Phone: +385 (51) 770 447
Fax: +385 (51) 686 166
www.intechopen.com

InTech China
Unit 405, Office Block, Hotel Equatorial Shanghai
No.65, Yan An Road (West), Shanghai, 200040, China
中国上海市延安西路65号上海国际贵都大饭店办公楼405单元
Phone: +86-21-62489820
Fax: +86-21-62489821

IntechOpen